Design and Synthesis of Heterostructured Quantum Dots with Dual Emission in the Visible and Infrared

Qianglu Lin,[†,‡] Nikolay S. Makarov,[†] Weon-kyu Koh,[†] Kirill A. Velizhanin,[†] Claudiu M. Cirloganu,[†] Hongmei Luo,[‡] Victor I. Klimov,[†] and Jeffrey M. Pietryga*[,†]

[†]Center for Advanced Solar Photophysics, Los Alamos National Laboratory, Los Alamos, New Mexico 87545, United States and [‡]Department of Chemical and Materials Engineering, New Mexico State University, Las Cruces, New Mexico 88003, United States

ABSTRACT The unique optical properties exhibited by visible emitting core/shell quantum dots with especially thick shells are the focus of widespread study, but have yet to be realized in infrared (IR)-active nanostructures. We apply an effective-mass model to identify PbSe/CdSe core/shell quantum dots as a promising system for achieving this goal. We then synthesize colloidal PbSe/CdSe quantum dots with shell thicknesses of up to 4 nm that exhibit unusually slow hole intraband relaxation from shell to core states, as evidenced by the emergence of dual emission, *i.e.*, IR photoluminescence from the PbSe core observed simultaneously with visible emission from the CdSe shell. In addition to the large shell thickness, the development of slowed intraband relaxation is facilitated by the existence of a sharp core–shell interface without discernible alloying. Growth of thick shells without interfacial alloying or incidental formation of homogeneous CdSe nanocrystals was accomplished using insights attained *via* a systematic study of the dynamics of the cation-exchange synthesis of both PbSe/CdSe and the related system PbS/CdS. Finally, we show that the efficiency of the visible photoluminescence can be greatly enhanced by inorganic passivation.

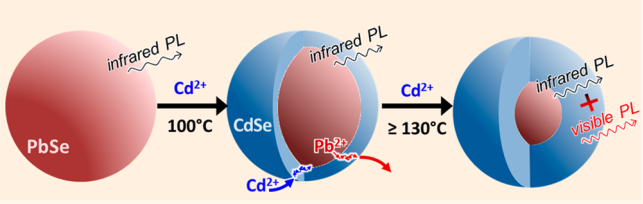

KEYWORDS: quantum dots · core/shell nanocrystal · dual emission · cation exchange · vacancy formation · effective-mass model

Core/shell structures have become ubiquitous in the field of colloidal quantum dots (QDs). Devised originally for improving emission quantum yields (QYs) and QD stability,[1] core/shell approaches have evolved to allow for manipulating carrier recombination dynamics and band gap energies[2,3] and even the strength and sign of exciton–exciton interaction.[4,5] Compared to core-only or thin-shell ("standard") nanocrystals, QDs with very thick shells (in the case of CdSe/CdS often referred to as "giant" QDs or g-QDs[6]) exhibit a number of novel and useful properties, such as nearly blinking-free single-QD emission, suppressed Auger recombination,[7] and a large effective Stokes shift between photoluminescence (PL) and the onset of strong optical absorption. To date, it has been demonstrated that these characteristics can be exploited to allow superior performance in a range of applications, including in subdiffraction-limit imaging,[8] in three-dimensional optical tracking,[9] and most recently in luminescent solar concentrators.[10]

This material combination also provides unique opportunities for manipulating carrier dynamics through structural control. The optical absorption at high energies of CdSe/CdS QDs with very thick shells,[6] and in the related CdSe/CdS dot/rod nanocrystals as well,[11] is dominated by shell-based states. Further, the quasi-type II energy structure, with a small energy offset between the core and shell conduction bands, means that while band-edge electrons remain delocalized throughout the entire nanocrystal, band-edge holes are localized only in the CdSe core.[7,12,13] Intriguingly, the rate of relaxation of holes from CdS- to CdSe-based states is strongly influenced by the structure

* Address correspondence to pietryga@lanl.gov.

Received for review October 10, 2014 and accepted November 26, 2014.

Published online November 26, 2014
10.1021/nn505793y

of the core/shell interface. This can most clearly be seen in the contrasting properties of g-QD-like CdSe/CdS QDs featuring an intentionally alloyed interface[14] and those of so-called "dot-in-bulk" (DiB) nanocrystals, in which the interface features a selective energetic barrier in the valence band associated with a thin zinc-blende CdS layer separating the zinc-blende CdSe core from the thick wurtzite CdS shell.[15] Because of this barrier, relaxation of "hot" holes from the shell to the core in DiB nanocrystals is dramatically slowed, to the point at which radiative recombination from high-lying shell-based states becomes competitive. The definitive evidence of this effect is two-color (or dual) emission under both low-intensity optical and electrical excitation,[16] which is evidence of a greatly reduced rate of cooling for shell-localized "hot" holes. On the other hand, the insertion of a CdSeS alloy layer at the interface of QDs with equally thick shells reduces this barrier, restoring fast intraband hole relaxation to the core and eliminating hot emission.

Much less explored is the utilization of these thick-shell motifs in the infrared (IR), which would have uniquely important technological benefits. For instance, suppressing Auger recombination could improve the performance of devices based on IR QDs, such as light-emitting diodes[17,18] or solar cells[19−22] (particularly when using concentrated sunlight[23]). At the same time, near-IR-emitting QDs with large Stokes shifts could enable luminescent solar concentrators capable of harvesting a larger fraction of the solar spectrum than those based on visible-emitting QDs.[10] The realization of slow carrier cooling in IR QDs may also give rise to additional opportunities. As fluorophores, dual-emitting QDs in which at least one of the colors is in the IR would potentially enable entirely new concepts in optical communications, nanoscale light sources, and biolabeling. A recent phenomenological model[24] also suggests that slowing carrier cooling is a viable approach to improving the efficiency of "carrier multiplication" (CM), a process that can boost the efficiency of solar cells based on IR QDs by producing additional current from high-energy photons.[23,25]

While identifying potential avenues toward the realization of this phenomenon in an IR QD, our focus naturally turned to the lead chalcogenides, and PbSe in particular, as a starting point. PbSe QDs offer efficient and widely tunable IR emission[26−28] and are amenable to cation exchange by treatment with Cd^{2+} ions to produce very stable PbSe/CdSe core/shell QDs with efficient IR PL.[29] Similar to the CdSe/CdS QDs discussed above, PbSe/CdSe QDs have been described as featuring a quasi-type II energy structure, with a small energy offset between the core and shell conduction bands and a much larger offset between respective valence bands (nearly equal to the band gap difference between CdSe and PbSe).[29,30] While earlier works on PbSe/CdSe QDs[30−33] have not reported dual emission, more recent studies of CM in these structures have indicated a dramatic increase in the multiexciton yield at large shell thicknesses, which was accompanied by the development of a shell-related PL band[34] consistent with slowed cooling of shell-localized holes.

Motivated by these initial results, here, we performed numerical modeling of electronic states in PbSe/CdSe QDs. This theoretical analysis revealed two key features emerging at large shell thicknesses that could potentially lead to slow hole cooling: (1) a vanishingly small spatial overlap between shell-based higher-energy hole states and low-lying core-based levels and (2) a sizable energetic gap separating a dense quasi-continuum of shell-based hole states from sparse core-localized levels. Calculations further suggested that these attributes require a sharp boundary at the core/shell interface. With the goal of realizing the desired shell thickness experimentally, we then conducted a systematic experimental study of the cation-exchange synthesis of both PbSe/CdSe and PbS/CdS QDs, complemented by a quantitative analysis of shell-growth dynamics. This exercise produced important guidelines for the creation of shell thicknesses of up to 4 nm without the formation of homogeneous CdSe (or CdS) nanocrystals and with retention of abrupt core/shell interfaces. As predicted by the modeling, we find that at shell thicknesses above 1.5 nm a second emission channel at visible energies indeed emerges, which can be attributed to recombination involving high-lying shell-based hole states. We also demonstrate that inorganic passivation through ZnS-shell growth greatly enhances this visible emission, which further supports that it arises from states within the QD band structure rather than from surface traps, as observed in previous reports of PbS/CdS QDs.[35]

RESULTS AND DISCUSSION

To calculate electronic states in PbSe/CdSe QDs, we apply an effective-mass formalism implemented using a mesh-based method of solving the radial Schrödinger equation. This is done *via* discretization of the radial coordinate on the mesh, which transforms the Schrödinger equation into a generalized matrix eigenvalue problem. We have found that this approach is surprisingly fast in terms of computational time and free of numerical instabilities. To account for the complexity of the PbSe/CdSe interface arising from the difference in the positions of band minima within the Brillouin zone, we have used transfer-matrix-based boundary conditions with matrix elements derived from the comparison between the calculated and the measured energies of the band-edge transition for a series of PbSe/CdSe QD samples (see "Theoretical methods" in the Supporting Information for details of our calculations).

In Figure 1, we model electronic states in QDs with a total radius R = 4 nm as a function of CdSe shell thickness, H. The calculations show that the energies of

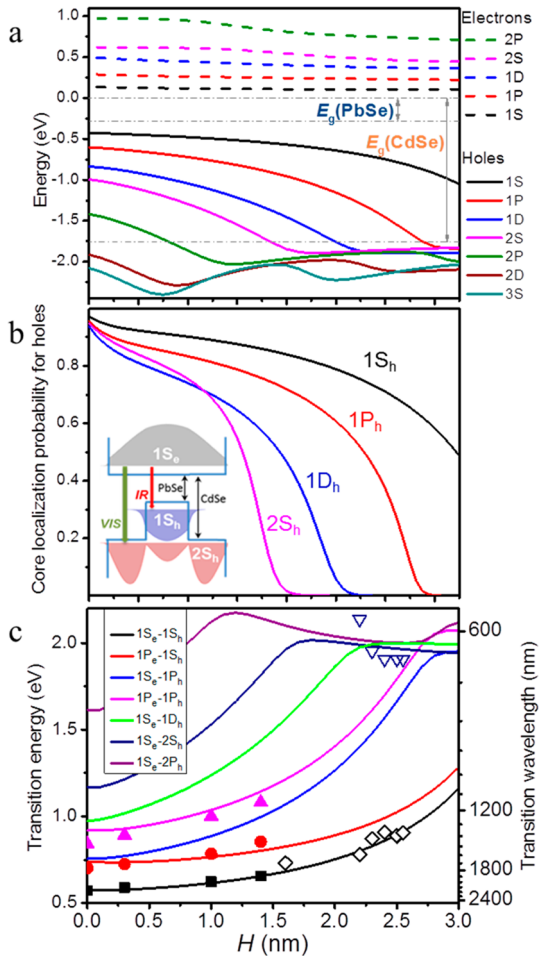

Figure 1. Calculated dependence of band structure parameters of PbSe/CdSe QDs on shell thickness, *H*, for QDs of total radius 4 nm. (a) *H*-dependence of the energy (relative to the bulk conduction band minimum) of the lowest-lying electron (dashed lines) and hole (solid) states. (b) *H*-dependence of the core localization probability for the lowest-lying hole states; inset depicts the calculated modulus squared of the radial wave functions of $1S_e$, $1S_h$, and $2S_h$ states ($H = R/2$), highlighting the different localizations exhibited by each state, with green and red arrows representing the recombination pathway for visible and IR PL, respectively. (c) *H*-dependence of the energies of several transitions potentially contributing to QD absorption and/or PL; symbols are extracted peak positions from IR absorption (solid symbols; see Supporting Figure S6 for complete spectra), IR PL (open diamonds), and visible PL (open triangles) spectra of sequential shell thicknesses during cation exchange of 4 nm QDs performed at 130 °C.

the first few electron levels are very similar and vary only weakly with *H* (Figure 1a), in stark contrast to the behavior of the hole states, which quickly shift up in energy. Important differences are also seen in the localization of electron and hole states. As expected for a quasi-type II QD, electron states remain delocalized over the entire QD regardless of *H*. On the other hand, as shown in Figure 1b, the core localization probability of the four lowest hole states changes dramatically with *H*, with the higher-lying states expelled from the core one-by-one as shell thickness increases. For $H > 2$ nm, only two widely separated levels, $1S_h$ and $1P_h$, remain in the core, while the others contribute to a dense quasi-continuum of states above the CdSe band edge (Figure 1a). The combination of both energetic and spatial separation between this collection of largely shell-localized hole states and the lower-lying core-based states (see spatial distributions of the $1S_h$ and $2S_h$ wave functions for $H = R/2$; inset of Figure 1b) can be expected to facilitate the reduction in the rate of phonon-mediated cooling necessary for activating a high-energy emission channel.

This analysis suggests that dual emission is not typically seen in PbSe/CdSe QDs because it requires very thick shells that have proven unattainable *via* cation exchange performed at moderate temperatures (≤100 °C). While it has been shown that the extent of cation exchange is temperature dependent,[29] use of even higher reaction temperatures carries potential complications. The band structures calculated above rely on an abrupt core/shell interface; in fact, further calculations show that, just as in CdSe/CdS QDs, structures featuring an interfacial alloy layer (in this case, a $Pb_{1-x}Cd_xSe$ layer between the PbSe core and CdSe shell) will likely not exhibit slow intraband hole relaxation (see Supporting Figure S2). For CdSe shells grown at low temperatures (<100 °C) no clear evidence of such an alloy has ever been reported.[29,32,33] In bulk films, however, the solubility of CdSe in PbSe increases with temperature,[36] an effect that could be exacerbated in nanocrystals due to their ability to accommodate strain; thus, some degree of alloying can potentially occur at the high temperatures necessary to achieve thicker shells. This suggests that while the sparser distribution of hole states seen in PbSe/CdSe QDs with an abrupt interface can be expected to lead to slow phonon-mediated hole cooling,[37] potentially allowing dual emission and/or enhanced CM,[34] even the introduction of a thin intermediate alloy layer will likely result in typically fast intraband relaxation.[38]

Accordingly, pursuant to our attempts to create PbSe/CdSe QDs with thick CdSe shells, we sought to establish experimentally the relationship between ion-exchange temperature and achievable shell thickness. Previous studies of ion exchange in PbSe/CdSe structures depict this process in terms of the temperature-dependent formation of vacancies or vacancy–interstitial pairs.[31] To probe the dynamics of this process, we performed temperature-controlled Cd exchange on PbSe QDs of total radius $R = 3.5$, 4.1, 4.8, and 6.6 nm.[29] The exchange was initiated by adding excess Cd-oleate to purified PbSe QDs at room temperature and then heating sequentially to 100, 130, 150, and finally 200 °C. Shell growth was monitored by a combination of transmission electron microscopy (TEM, Figure 2a and Supporting Figures S16–S20), PL spectroscopy (Figure 2b), and elemental analysis by inductively coupled plasma optical emission spectroscopy

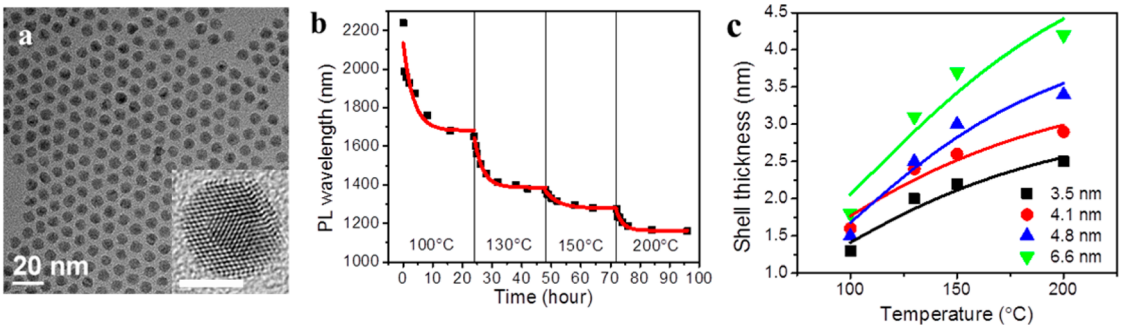

Figure 2. (a) TEM image of PbSe/CdSe QDs with 2.7 nm core radius and 1.3 nm shell thickness after 24 h reaction time at 100 °C. Inset is a high-resolution image of the same QDs (scale bar is 5 nm), showing a distinct ("sharp") core/shell interface. (b) Temporal evolution of PL wavelength peak of PbSe/CdSe QDs (total radius R = 4.1 nm) during cation exchange at several temperatures sequentially (red line shows the exponential fit according to our kinetic model). (c) Temperature-dependent CdSe saturation shell thickness (by TEM) for the PbSe/CdSe QDs with R = 3.5 nm (black), 4.1 nm (red), 4.8 nm (blue), and 6.6 nm (green). Solid lines show fits according to our thermodynamic model (see Supporting Information for details).

(ICP-OES, Supporting Table S1) performed on aliquots during reaction.

We observed that at each reaction temperature a "saturation" shell thickness is reached after ~16 to 24 h of reaction (Figure 2b,c). In control experiments with smaller QDs (R < 2.5 nm) complete conversion was observed at or above 180 °C,[32] while prolonged heating (>4 h) at 200 °C of bigger QDs led to the formation of very small, homogeneous CdSe nanoparticles (Supporting Figure S20) through delamination of the shell from the core in a manner similar to that observed during vacuum annealing of PbSe/CdSe QDs.[39]

The observed saturation behavior is consistent with the earlier proposed model of vacancy-assisted ion exchange.[31] Given that the vacancy formation enthalpy in bulk CdSe[40] is significantly higher than that in PbSe,[41] it is reasonable to assume that exchange at any temperature will be limited by the generation of vacancies in the CdSe through which the exchanged ions diffuse. While the vacancy generation rate (per unit volume) should be higher in these nanoparticles than in the bulk, it should decrease as the CdSe shell gets thicker, because the vacancy formation energy (~3 eV in bulk CdSe)[40] scales with the material melting point,[42] which in turn scales with particle (or domain) size.[43] Thus, at constant temperature, diffusion through an increasingly thick CdSe shell would be expected to get slower and slower until net replacement seems to essentially stop, at which point a saturation shell thickness is reached. Increasing the temperature boosts the vacancy generation rate, allowing diffusion over a longer core-to-surface distance and reactivating the replacement process.

To consider the empirical energetics of the process, we describe the ion exchange reaction with the following equation:

$$\text{Cd-oleate}_{(sol)} + \text{PbSe}_{(s)} \rightarrow \text{CdSe}_{(s)} + \text{Pb-oleate}_{(sol)} \quad (1)$$

By considering saturation to represent an effective reaction equilibrium, we can estimate the energy, ΔE, involved in a single ion replacement by evaluating the following expression:

$$\Delta G = 0 = \frac{\Delta E}{k_B} + T\ln(\gamma^{o}N^{o}_{Pb}) - T\ln(\gamma^{i}N^{i}_{Pb}) + T\ln(\gamma^{i}N^{i}_{Cd}) - T\ln(\gamma^{o}N^{o}_{Cd}) \quad (2)$$

where N represents the number of Pb (subscript Pb) and Cd (subscript Cd) ions inside (superscript i) or outside (superscript o) of the QD for a given temperature at saturation, and γ is the respective activity coefficient. Rearranging this expression with some simplifying approximations based on our conditions (see Supporting Information for details), we arrive at the following relationship between the QD geometrical parameters (total radius, R, and core radius, r) and the reaction temperature:

$$\ln\frac{(R^3 - r^3)^2}{r^3} = C - \frac{\Delta E}{k_B T} \quad (3)$$

A plot of the left-hand side of eq 3 at each saturation point *vs* $-1/T$ yields a line with a slope of $\Delta E/k_B$ (Supporting Figure S4). The average value of this energy for all studied PbSe/CdSe QD samples is 0.44 ± 0.06 eV, with no notable size dependence, which is similar to that found for PbS/CdS cation exchange (ΔE = 0.52 eV, Supporting Figure S11). The derived value of ΔE is significantly smaller than the vacancy formation energy for bulk CdSe,[40] which is consistent with expectations for nanosized shells of CdSe with a relatively high surface-to-volume ratio. In addition, the surface geometry of these quasi-spherical QDs, which comprises numerous relatively small faces and a relatively high density of edges compared to, for example, cube-shaped QDs,[31] can produce further deviation from the bulk energy prediction. As vacancy formation energy can vary for different crystal faces of the same lattice,[44] it can be expected that ion exchange will be especially favorable at specific sites distributed across the QD surfaces. The result would be an even lower average energy of exchange and a preservation

(on average) of the quasi-spherical shape in the shrinking PbSe core (see Supporting Figures S17−S19).

Although saturation thicknesses in PbSe- and PbS-based QDs are similar, they are reached much more quickly at any given temperature in the sulfide case. To analyze the kinetics of this process, we use a saturation-based model that assumes exchange occurs at only a fixed number of possible replacement sites at a given temperature (potentially due to limits of ion diffusion, as described above), which are "consumed" according to a first-order reaction rate constant. From above, the number of potential cation-exchange sites available at a given temperature is N^{i}_{Cd}. If we follow the progress of reaction in terms of the number, N, of actually exchanged sites at any given time before saturation is reached, we can use the following expression for the rate of reaction, r_{rxn}, to derive a rate constant, k:

$$r_{rxn} = \frac{dN}{dt} = k(N^{i}_{Cd} - N) \quad (4)$$

or

$$\ln(N^{i}_{Cd} - N) = -kt + \text{const} \quad (5)$$

For any temperature, N^{i}_{Cd} is simply the volume of the CdSe shell at "saturation" multiplied by the number of cations per unit volume (according to the crystal structure). We can derive N at any given time from the shell thickness of a reaction aliquot, which was inferred from the peak energy of the IR PL (see correlation between spectroscopic and other methods for shell-thickness determination in Supporting Figure S3). By plotting $\ln(N^{i}_{Cd} - N)$ as a function of reaction time, t, at a given temperature, we can extract a reaction rate constant from the slope of the linear fit. In this way, we derive apparently temperature-independent rate constants of 0.20 ± 0.02 h^{-1} for the selenide system (Supporting Figure S5) and 0.28 ± 0.02 h^{-1} for the sulfide (Supporting Figure S12). While the lack of dependence on temperature of these rates seems counterintuitive, we believe that it arises because our rate constants are expressed in terms of a fixed number of exchange sites, N_e, which already captures temperature-dependent changes in diffusion rates. The difference in rates between the sulfide and selenide systems, which is the reverse of their vacancy formation energies for parental bulk semiconductors, might be explained by the metastability of zinc-blende CdS[45] that could result in undetectable polytypism, leading to either high defect concentrations (including vacancies) or a greater degree of Cd diffusion *via* interstitial sites, such as has been noted in CdS thin films studied under Cd-rich conditions.[46]

The temperature-dependent studies above yield important conclusions to guide our attempts to achieve QDs with discernible shell-based emission. First, shell thicknesses of interest (H > 2 nm) can be achieved at reaction temperatures only moderately higher than used previously,[29] in this case 130−150 °C, as long as the initial PbSe QDs are of radius ≥4 nm. Second, consistent with all previous reports of cation exchange at lower temperatures, no evidence of alloying between core and shell is seen in any sample, although the very similar lattice parameter of the two cubic domains (Δa = 1.1%) greatly reduces the chance of directly observing signatures of alloy-induced strain relaxation such as has been probed using Raman spectroscopy in other systems.[47] High-resolution TEM images of all samples contain numerous QDs in which an abrupt demarcation between core and shell lattices is clearly observed (Supporting Figures S16−S20). Indeed, at the highest temperatures (200 °C), far from alloying, the CdSe and PbSe domains began to physically separate, producing very small CdSe nanocrystals (Supporting Figure S20), suggesting a strong resistance to alloying in nanoscale combinations of these materials. This is perhaps due to the incompatibility between the different coordination numbers found in the rock-salt (six) and zinc-blende (four) structures of PbSe and CdSe domains, respectively.

Accordingly, we focused our efforts on thick-shell QDs of R = 4 nm produced by cation exchange carried out at 130 °C. Figure 3 shows the evolution of key optical characteristics during formation of sequentially thicker shells during a single continuous reaction. As the shell thickness increases, peaks corresponding to distinct excitonic transitions in the QD absorption spectra (Figure 3a) blue-shift, in excellent agreement with the predictions of our model (Figure 1c; solid symbols), but also become progressively broader and weaker, as expected for a transition to a quasi-type-II localization regime. As previously observed, growth of a CdSe shell results in a dramatic increase in IR PL quantum yield[29] and a lengthening of IR PL lifetime[48] (Figure 3b,d and Supporting Table S2), which is also consistent with quasi-type-II localization. Similar trends are observed during growth of PbS/CdS QDs (Supporting Figures S13, S14).

At H > 1.5 nm, we typically observe the emergence of visible emission. Initially, at smaller shell thicknesses, excitation at 400 nm produces a weak, broad band that peaks at ∼500 nm (Figure 3c). As shell growth continues, this feature red-shifts and narrows until it reaches ∼650−680 nm at H = 2.5 nm, and the visible PL QY increases by a factor of more than 20 to ∼0.1%. The apparent size dependence of the PL energy for QDs with thicker shells, which remains higher than the bulk band gap of CdSe (1.75 eV), suggests the involvement of quantum-confined states within the QD band structure. At the same time, the dependence of the visible PL QY on shell thickness supports the assertion that radiative recombination competes with intraband hole cooling, which as our model predicts, gets progressively slower as the shell gets thicker.

To further support this assignment, we conducted preliminary experiments in inorganic passivation to

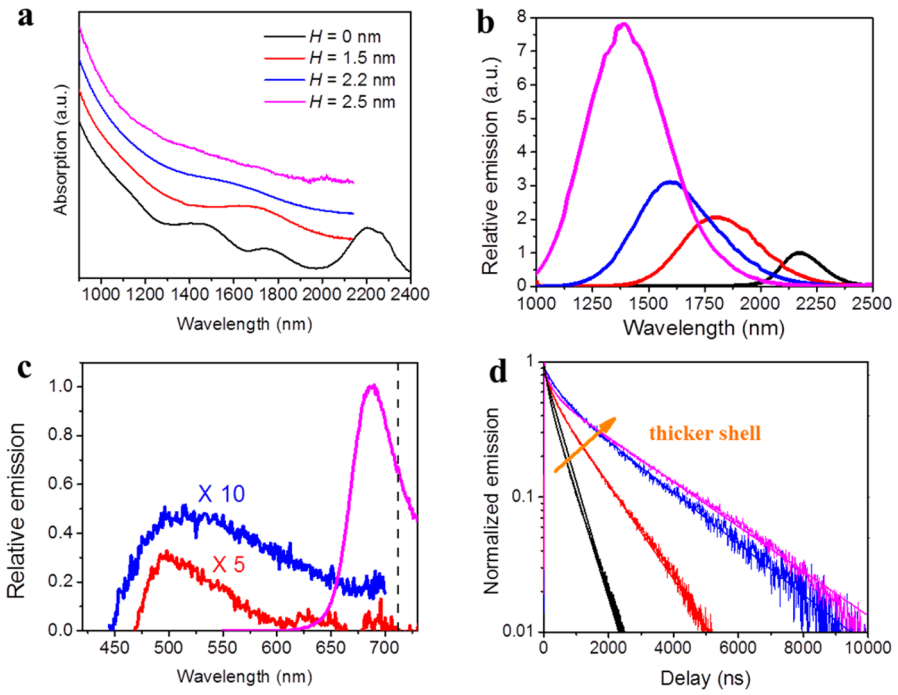

Figure 3. (a) Absorption spectra of the PbSe/CdSe core/shell QDs (R = 4.0 nm) with shell thickness, H, varying from 0 (black) to 2.5 nm (magenta). (b) Corresponding IR photoluminescence (PL) spectra showing core-based emission; QYs increase with H, for this series up to QY = 6%. (c) Relative visible PL spectra from the same QDs; red and blue traces are scaled vertically by the indicated factor, with a PL QY for H = 2.5 (magenta) of 0.1%; the dashed line represents the bulk band gap of CdSe. (d) IR PL decay traces of PbSe/CdSe core−shell QDs of varying H.

discern its effect on the efficiency of the visible emission. We find that even nonoptimized growth of a very thin (not fully discernible *via* TEM, Supporting Figure S22) shell of either ZnS (Figure 4) or CdS resulted in an up to 4-fold enhancement of the visible PL QY, further demonstrating that the hot emission from the CdSe shell is not surface trap-mediated.

Visible emission is also observed from PbS/CdS QDs when shell thickness exceeds 1.5 nm, starting as a broad, weak feature spanning ~400−600 nm (Supporting Figure S15). In contrast to the PbSe/CdSe emission, a significant portion of the PbS/CdS PL spectrum extends into the spectral region below the CdS band gap, suggesting the involvement of intragap defects. This is similar to the trap-mediated emission seen in CdS QDs[49] and in a previous report on PbS/CdS core/shell QDs.[35]

Our effective-mass calculations of the PbSe/CdSe QD band structure as a function of H (Figure 1c) help identify the origin of the visible emission feature. As expected, the energies of the IR PL (open diamonds) at each shell thickness match the calculated value for the $1S_e-1S_h$ transition energy (solid black line). The energy of the visible PL band (open triangles) for QDs with shell thicknesses between 2.2 and 2.7 nm is near the energies of three closely spaced transitions, $1S_e-2S_h$, $1S_e-1D_h$, and $1S_e-2P_h$ (dark blue, green and purple lines, respectively); however, because of optical selection rules, the dominant contribution is likely from the first one ($1S_e-2S_h$), which involves states of the same

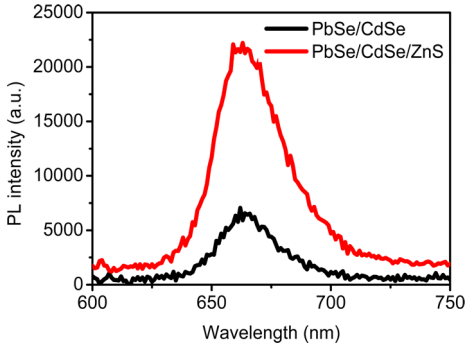

Figure 4. Growth of a very thin (<0.3 nm) ZnS shell on a PbSe/CdSe QD (r = 3.5 nm, H = 2.0 nm) strongly enhances visible PL QY.

symmetry. Importantly, as shown in the inset of Figure 1b, in thick-shell PbSe/CdSe QDs, the $2S_h$ hole wave function resides primarily in the shell. The reduced overlap between this wave function and that of the core-based band-edge hole state ($1S_h$), combined with the large energy gap between the shell and the core levels, leads to suppressed hole cooling and, as a result, a considerable increase in the intensity of shell emission in the visible originating from radiative recombination of "unrelaxed" shell-localized holes.

Using our model we can also assign some intermediate transitions located between the energies of IR and visible emission bands. Specifically, in absorption spectra of thinner-shell samples (Supporting Figure S6) in addition to the band-edge peak (solid squares in

Figure 1c) we can also resolve two higher-energy features (red and magenta symbols in Figure 1c). The second feature is close to our calculations for the $1P_e-1S_h$ transition, which is nominally parity forbidden but is also observed in core-only PbSe and PbS QDs.[50] On the basis of our calculations, the third absorption feature is likely due to a parity-allowed $1P_e-1P_h$ transition.

The close correspondence between calculated and measured energies of optical transitions observed in both PL and absorption spectra provides strong corroboration of our model. Although our selection of boundary conditions was based solely on the size dependence of the experimentally determined energy for the lowest $1S_e-1S_h$ feature, it allows accurate prediction of the visible emission wavelength as well as the energies of higher-lying transitions involving not only ground but also excited electronic states.

CONCLUSIONS

We have demonstrated that the uniquely advantageous optical characteristics of the widely studied visible-emitting thick-shell QDs can be extended into the IR using thick-shell PbSe/CdSe and PbS/CdS core/shell QDs. With the guidance of a systematic study of the dynamics of the cation-exchange synthesis route, we were able to identify conditions for the preparation of QDs with shells up to 4 nm thick (*ca.* 13 CdSe monolayers) without discernible core–shell interfacial alloying or formation of homogeneous CdSe (CdS) particles. Consistent with the results of effective-mass calculations that predict a sizable energetic gap between the core- and the shell-based valence-band levels, these QDs exhibit markedly suppressed relaxation of holes from the core to the shell states. This is manifested in dual-band PL with visible and IR bands, both of which are size-tunable. Finally, the visible PL QY can be greatly improved by growth of even a very thin passivating layer of ZnS or CdS. These nanoheterostructures are an example of a unique class of tunable, dual-emitting, dispersible fluorophores that may be useful for unique types of labeling and PL microscopy, especially when the IR emission falls within the tissue transparency optical window. This type of structure-based control over carrier relaxation may also prove useful for "hot-carrier" photovoltaics or for improving the efficiencies of desirable processes that compete with cooling, such as CM. Indeed, while the above-described QDs have demonstrated enhanced CM efficiency relative to standard core-only PbSe QDs,[34] the potential generalization of these concepts may even allow efficient CM to be induced in heterostructures combining as-of-yet nominally non-CM-active materials.

EXPERIMENTAL METHODS

General Considerations. Oleic acid (OA, technical grade 90%), lead(II) oxide (99.999%), cadmium oxide (99.998%), and selenium shot (99.999%) were purchased from Alfa Aesar; 1-octadecene (ODE, technical grade 90%), bis(trimethylsilyl)sulfide (95%), cadmium cyclohexanebutyrate (24% Cd), bis(trimethylsilyl)sulfide (TMS_2S, 95%), oleylamine (80–90%), and sulfur (99.5%) were purchased from Acros Organics; tributylphosphine (97%) was purchased from Sigma-Aldrich; trioctylphosphine (TOP, 97%) and diisobutylphosphine (97%) were purchased from Strem. Trioctylphosphine selenide (TOPSe) solutions were prepared by heating the appropriate amounts of selenium shot and TOP at 100 °C with stirring until a clear solution was obtained. All syntheses and purifications were performed under air-free conditions using a combination of Schlenk-line and glovebox techniques.

Synthesis of Pristine *R* = 4.8 nm PbSe QDs. Pb-oleate precursor was prepared by heating a solution containing 0.892 g of PbO, 4 mL of OA, and 16 mL of ODE to 120 °C under vacuum for 30 min. Then the solution was purged with argon and heated to 180 °C. A syringe containing 50 μL of diisobutylphosphine and 1 mL of 2 M TOPSe was rapidly injected. The solution was then cooled to 160 °C for 8 min. To collect and purify the QDs, excess ethanol was added to the solution to precipitate QDs, and the precipitate was redissolved in toluene.

Pristine *R* = 3.5, 4.0, 4.1, and 6.6 nm PbSe QDs were prepared in a similar way except with a reaction time at 160 °C of 2, 4, 5, and 30 min, respectively.

Synthesis of Pristine *R* = 3.7 nm PbS QDs. Pb-oleate precursor was prepared by heating a solution containing 0.892 g of PbO, 4 mL of OA, and 16 mL of ODE to 120 °C under vacuum for half an hour. Then the solution was purged with argon and heated to 220 °C. A syringe containing 50 μL of bis(trimethylsilyl)sulfide and 1 mL of 2 M TOPS was rapidly injected. The solution was then cooled to 180 °C for 5 min. Finally, the reaction was quenched by removing from heat, and the QDs were collected and purified as described above.

CdSe or CdS Shell Growth. A three-neck flask containing 1.28 g of CdO, 10 mL of OA, and 10 mL of ODE was heated to 260 °C for 30 min to form a clear solution. Then the solution was placed under vacuum at 120 °C for 1 h to remove water. A PbSe or PbS QD solution in toluene was then added to the Cd-oleate solution at room temperature, and the toluene was subsequently removed under vacuum. Cation exchange was performed at 130 °C for 18 h to achieve a 2.5 nm thick shell. Reaction progress was monitored by determining the shell thickness of QDs in small aliquots taken periodically. After the desired shell thickness was reached, the QDs were collected and purified as described above.

ZnS Shell Growth on PbSe/CdSe QDs. Zn precursor solution (0.1 M) was prepared by dissolving 1 mmol of zinc acetate in 10 mL of OLA. Sulfur precursor (0.05 M) was prepared by mixing 0.1 mL of TMS_2S in 9.5 mL of OLA. A solution containing purified PbSe/CdSe QDs was loaded into a three-neck flask containing 1 mL of OLA, 4 mL of ODE, and 0.1 mL each of the Cd and S precursor solutions. The mixture was heated to 100 °C in a vacuum to remove the QD solvent. The reaction was then carried out at 130 °C for 1 h, and the QDs collected and purified as described above.

Characterization of QDs. Transmission electron microscope (TEM) and high-resolution TEM (HR-TEM) images were taken using a JEOL 2010 TEM on drop-cast samples on carbon-coated copper grids. Absorption spectra were measured by a PerkinElmer Lambda 950 spectrophotometer. Visible PL spectra were recorded using a Horiba Scientific FluoroMax-4 spectrofluorometer using 400 nm excitation. Infrared PL spectra were taken using a home-built setup: excitation was provided by an 808 nm laser, and emission was analyzed using a grating monochromator and an LN2-chilled InSb detector. The photoluminescence quantum yields were determined relative to LDS-698

reference dye (in methanol, QY = 0.41) for visible PL and to IR-26 (in 1,2-dicholorethane, QY = 0.0005) for IR PL. Pb:Cd ratios were determined by elemental analysis using a Shimadzu ICPE-9000 ICP-OES.

Conflict of Interest: The authors declare no competing financial interest.

Supporting Information Available: Detailed descriptions of characterization, modeling methods, additional TEM images, and details of PbS/CdS experiments. This material is available free of charge *via* the Internet at http://pubs.acs.org

Acknowledgment. W.-k.K., K.A.V., C.M.C., V.I.K., and J.M.P. acknowledge the support of the Center for Advanced Solar Photophysics (CASP), an Energy Frontier Research Center funded by the U.S. Department of Energy, Office of Science, Office of Basic Energy Sciences. N.S.M. is a CASP member supported by LANL Director's Postdoctoral Fellowship. Q.L. and H.L. are CASP affiliates supported by the New Mexico Consortium and Los Alamos National Laboratory.

REFERENCES AND NOTES

1. Hines, M. A.; Guyot-Sionnest, P. Synthesis and Characterization of Strongly Luminescing ZnS-Capped CdSe Nanocrystals. *J. Phys. Chem.* **1996**, *100*, 468–471.
2. Kim, S.; Fisher, B.; Eisler, H.-J.; Bawendi, M. Type-II Quantum Dots: CdTe/CdSe (core/shell) and CdSe/ZnTe (core/shell) Heterostructures. *J. Am. Chem. Soc.* **2003**, *125*, 11466–11467.
3. Balet, L. P.; Ivanov, S. A.; Piryatinski, A.; Achermann, M.; Klimov, V. I. Inverted Core/Shell Nanocrystals Continuously Tunable between Type-I and Type-II Localization Regimes. *Nano Lett.* **2004**, *4*, 1485–1488.
4. Ivanov, S. A.; Nanda, J.; Piryatinski, A.; Achermann, M.; Balet, L. P.; Bezel, I. V.; Anikeeva, P. O.; Tretiak, S.; Klimov, V. I. Light Amplification Using Inverted Core/Shell Nanocrystals: Towards Lasing in the Single-Exciton Regime. *J. Phys. Chem. B* **2004**, *108*, 10625–10630.
5. Klimov, V. I.; Ivanov, S. A.; Nanda, J.; Achermann, M.; Bezel, I.; McGuire, J. A.; Piryatinski, A. Single-Exciton Optical Gain in Semiconductor Nanocrystals. *Nature* **2007**, *447*, 441–446.
6. Chen, Y.; Vela, J.; Htoon, H.; Casson, J. L.; Werder, D. J.; Bussian, D. A.; Klimov, V. I.; Hollingsworth, J. A. "Giant" Multishell CdSe Nanocrystal Quantum Dots with Suppressed Blinking. *J. Am. Chem. Soc.* **2008**, *130*, 5026–5027.
7. García-Santamaría, F.; Chen, Y.; Vela, J.; Schaller, R. D.; Hollingsworth, J. A.; Klimov, V. I. Suppressed Auger Recombination in "Giant" Nanocrystals Boosts Optical Gain Performance. *Nano Lett.* **2009**, *9*, 3482–3488.
8. Lesoine, M. D.; Bhattacharjee, U.; Guo, Y.; Vela, J.; Petrich, J. W.; Smith, E. A. Subdiffraction, Luminescence-Depletion Imaging of Isolated, Giant, CdSe/CdS Nanocrystal Quantum Dots. *J. Phys. Chem. C* **2013**, *117*, 3662–3667.
9. Marchuk, K.; Guo, Y.; Sun, W.; Vela, J.; Fang, N. High-Precision Tracking with Non-blinking Quantum Dots Resolves Nanoscale Vertical Displacement. *J. Am. Chem. Soc.* **2012**, *134*, 6108–6111.
10. Meinardi, F.; Colombo, A.; Velizhanin, K. A.; Simonutti, R.; Lorenzon, M.; Beverina, L.; Viswanatha, R.; Klimov, V. I.; Brovelli, S. Large-Area Luminescent Solar Concentrators Based on 'Stokes-Shift-Engineered' Nanocrystals in a Mass-Polymerized PMMA Matrix. *Nat. Photonics* **2014**, *8*, 392–399.
11. Carbone, L.; Nobile, C.; De Giorgi, M.; Sala, F. D.; Morello, G.; Pompa, P.; Hytch, M.; Snoeck, E.; Fiore, A.; Franchini, I. R.; *et al.* Synthesis and Micrometer-Scale Assembly of Colloidal CdSe/CdS Nanorods Prepared by a Seeded Growth Approach. *Nano Lett.* **2007**, *7*, 2942–2950.
12. Lupo, M. G.; Della Sala, F.; Carbone, L.; Zavelani-Rossi, M.; Fiore, A.; Lüer, L.; Polli, D.; Cingolani, R.; Manna, L.; Lanzani, G. Ultrafast Electron–Hole Dynamics in Core/Shell CdSe/CdS Dot/Rod Nanocrystals. *Nano Lett.* **2008**, *8*, 4582–4587.
13. Zavelani-Rossi, M.; Lupo, M. G.; Tassone, F.; Manna, L.; Lanzani, G. Suppression of Biexciton Auger Recombination in CdSe/CdS Dot/Rods: Role of the Electronic Structure in the Carrier Dynamics. *Nano Lett.* **2010**, *10*, 3142–3150.
14. Bae, W. K.; Padilha, L. A.; Park, Y.-S.; McDaniel, H.; Robel, I.; Pietryga, J. M.; Klimov, V. I. Controlled Alloying of the Core–Shell Interface in CdSe/CdS Quantum Dots for Suppression of Auger Recombination. *ACS Nano* **2013**, *7*, 3411–3419.
15. Galland, C.; Brovelli, S.; Bae, W. K.; Padilha, L. A.; Meinardi, F.; Klimov, V. I. Dynamic Hole Blockade Yields Two-Color Quantum and Classical Light from Dot-in-Bulk Nanocrystals. *Nano Lett.* **2012**, *13*, 321–328.
16. Brovelli, S.; Bae, W. K.; Galland, C.; Giovanella, U.; Meinardi, F.; Klimov, V. I. Dual-Color Electroluminescence from Dot-in-Bulk Nanocrystals. *Nano Lett.* **2013**, *14*, 486–494.
17. Steckel, J. S.; Coe-Sullivan, S.; Bulović, V.; Bawendi, M. G. 1.3 to 1.55 μm Tunable Electroluminescence from PbSe Quantum Dots Embedded within an Organic Device. *Adv. Mater.* **2003**, *15*, 1862–1866.
18. Konstantatos, G.; Huang, C.; Levina, L.; Lu, Z.; Sargent, E. H. Efficient Infrared Electroluminescent Devices Using Solution-Processed Colloidal Quantum Dots. *Adv. Funct. Mater.* **2005**, *15*, 1865–1869.
19. Semonin, O. E.; Luther, J. M.; Choi, S.; Chen, H.-Y.; Gao, J.; Nozik, A. J.; Beard, M. C. Peak External Photocurrent Quantum Efficiency Exceeding 100% via MEG in a Quantum Dot Solar Cell. *Science* **2011**, *334*, 1530–1533.
20. Etgar, L.; Yanover, D.; Čapek, R. K.; Vaxenburg, R.; Xue, Z.; Liu, B.; Nazeeruddin, M. K.; Lifshitz, E.; Grätzel, M. Core/Shell PbSe/PbS QDs TiO_2 Heterojunction Solar Cell. *Adv. Funct. Mater.* **2013**, *23*, 2736–2741.
21. Park, H.-Y.; Ryu, I.; Kim, J.; Jeong, S.; Yim, S.; Jang, S.-Y. PbS Quantum Dot Solar Cells Integrated with Sol–Gel-Derived ZnO as an n-Type Charge-Selective Layer. *J. Phys. Chem. C* **2014**, *118*, 17374–17382.
22. Chuang, C.-H. M.; Brown, P. R.; Bulović, V.; Bawendi, M. G. Improved Performance and Stability in Quantum Dot Solar Cells through Band Alignment Engineering. *Nat. Mater.* **2014**, *13*, 796–801.
23. Hanna, M. C.; Beard, M. C.; Nozik, A. J. Effect of Solar Concentration on the Thermodynamic Power Conversion Efficiency of Quantum-Dot Solar Cells Exhibiting Multiple Exciton Generation. *J. Phys. Chem. Lett.* **2012**, *3*, 2857–2862.
24. Stewart, J. T.; Padilha, L. A.; Bae, W. K.; Koh, W.-K.; Pietryga, J. M.; Klimov, V. I. Carrier Multiplication in Quantum Dots within the Framework of Two Competing Energy Relaxation Mechanisms. *J. Phys. Chem. Lett.* **2013**, *4*, 2061–2068.
25. Klimov, V. I. Detailed-Balance Power Conversion Limits of Nanocrystal-Quantum-Dot Solar Cells in the Presence of Carrier Multiplication. *Appl. Phys. Lett.* **2006**, *89*, 123118.
26. Pietryga, J. M.; Schaller, R. D.; Werder, D.; Stewart, M. H.; Klimov, V. I.; Hollingsworth, J. A. Pushing the Band Gap Envelope: Mid-Infrared Emitting Colloidal PbSe Quantum Dots. *J. Am. Chem. Soc.* **2004**, *126*, 11752–11753.
27. Murray, C. B.; Sun, S.; Gaschler, W.; DoyLe, H.; Betley, T. A.; Kagan, C. R. Colloidal Synthesis of Nanocrystals and Nanocrystal Superlattices. *IBM J. Res. Dev.* **2001**, *45*, 47–56.
28. Evans, C. M.; Guo, L.; Peterson, J. J.; Maccagnano-Zacher, S.; Krauss, T. D. Ultrabright PbSe Magic-Sized Clusters. *Nano Lett.* **2008**, *8*, 2896–2899.
29. Pietryga, J. M.; Werder, D. J.; Williams, D. J.; Casson, J. L.; Schaller, R. D.; Klimov, V. I.; Hollingsworth, J. A. Utilizing the Lability of Lead Selenide to Produce Heterostructured Nanocrystals with Bright, Stable Infrared Emission. *J. Am. Chem. Soc.* **2008**, *130*, 4879–4885.
30. De Geyter, B.; Justo, Y.; Moreels, I.; Lambert, K.; Smet, P. F.; Van Thourhout, D.; Houtepen, A. J.; Grodzinska, D.; de Mello Donega, C.; Meijerink, A. The Different Nature of Band Edge Absorption and Emission in Colloidal PbSe/CdSe Core/Shell Quantum Dots. *ACS Nano* **2010**, *5*, 58–66.
31. Casavola, M.; van Huis, M. A.; Bals, S.; Lambert, K.; Hens, Z.; Vanmaekelbergh, D. Anisotropic Cation Exchange in

PbSe/CdSe Core/Shell Nanocrystals of Different Geometry. *Chem. Mater.* **2011**, *24*, 294–302.
32. Abel, K. A.; FitzGerald, P. A.; Wang, T.-Y.; Regier, T. Z.; Raudsepp, M.; Ringer, S. P.; Warr, G. G.; van Veggel, F. C. Probing the Structure of Colloidal Core/Shell Quantum Dots Formed by Cation Exchange. *J. Phys. Chem. C* **2012**, *116*, 3968–3978.
33. Bals, S.; Casavola, M.; van Huis, M. A.; Van Aert, S.; Batenburg, K. J.; Van Tendeloo, G.; Vanmaekelbergh, D. Three-Dimensional Atomic Imaging of Colloidal Core–Shell Nanocrystals. *Nano Lett.* **2011**, *11*, 3420–3424.
34. Cirloganu, C. M.; Padilha, L. A.; Lin, Q.; Makarov, N. S.; Velizhanin, K. A.; Luo, H.; Robel, I.; Pietryga, J. M.; Klimov, V. I. Enhanced Carrier Multiplication in Engineered Quasi-Type-II Quantum Dots. *Nat. Commun.* **2014**, *5*.
35. Zhao, H.; Chaker, M.; Wu, N.; Ma, D. Towards Controlled Synthesis and Better Understanding of Highly Luminescent PbS/CdS Core/Shell Quantum Dots. *J. Mater. Chem.* **2011**, *21*, 8898–8904.
36. Sealy, B. J.; Crocker, A. J. Some Physical Properties of the Systems $Pb_{1-x}Mg_xSe$ and $Pb_{1-x}Cd_xSe$. *J. Mater. Sci.* **1973**, *8*, 1247–1252.
37. Liu, C.; Peterson, J. J.; Krauss, T. D. Uncovering Hot Hole Dynamics in CdSe Nanocrystals. *J. Phys. Chem. Lett.* **2014**, 3032–3036.
38. Schaller, R. D.; Pietryga, J. M.; Goupalov, S. V.; Petruska, M. A.; Ivanov, S. A.; Klimov, V. I. Breaking the Phonon Bottleneck in Semiconductor Nanocrystals via Multiphonon Emission Induced by Intrinsic Nonadiabatic Interactions. *Phys. Rev. Lett.* **2005**, *95*, 196401.
39. Grodzińska, D.; Pietra, F.; van Huis, M. A.; Vanmaekelbergh, D.; de Mello Donegá, C. Thermally Induced Atomic Reconstruction of PbSe/CdSe Core/Shell Quantum Dots into PbSe/CdSe Bi-Hemisphere Hetero-Nanocrystals. *J. Mater. Chem.* **2011**, *21*, 11556–11565.
40. Van Vechten, J. Simple Theoretical Estimates of the Schottky Constants and Virtual-Enthalpies of Single Vacancy Formation in Zinc-Blende and Wurtzite Type Semiconductors. *J. Electrochem. Soc.* **1975**, *122*, 419–422.
41. Bublik, V. The Mean Square Atomic Displacements and Enthalpies of Vacancy Formation in Some Semiconductors. *Phys. Status Solidi A* **1978**, *45*, 543–548.
42. Ben-Abraham, S.; Rabinovitch, A.; Pelleg, J. Relations between Vacancy Migration and Formation Energies, Debye Temperature and Melting Point. *Phys. Status Solidi B* **1977**, *84*, 435–441.
43. Goldstein, A. N.; Echer, C. M.; Alivisatos, A. P. Melting in Semiconductor Nanocrystals. *Science* **1992**, *256*, 1425–1427.
44. Rempel, J. Y.; Trout, B. L.; Bawendi, M. G.; Jensen, K. F. Density Functional Theory Study of Ligand Binding on CdSe (0001), (000$\bar{1}$), and (11$\bar{2}$0) Single Crystal Relaxed and Reconstructed Surfaces: Implications for Nanocrystalline Growth. *J. Phys. Chem. B* **2006**, *110*, 18007–18016.
45. Yeh, C.-Y.; Lu, Z. W.; Froyen, S.; Zunger, A. Zinc-Blende–Wurtzite Polytypism in Semiconductors. *Phys. Rev. B* **1992**, *46*, 10086–10097.
46. Kumar, V.; Kröger, F. Self-Diffusion and the Defect Structure of Cadmium Sulfide. *J. Solid State. Chem.* **1971**, *3*, 387–400.
47. Tschirner, N.; Lange, H.; Schliwa, A.; Biermann, A.; Thomsen, C.; Lambert, K.; Gomes, R.; Hens, Z. Interfacial Alloying in CdSe/CdS Heteronanocrystals: A Raman Spectroscopy Analysis. *Chem. Mater.* **2012**, *24*, 311–318.
48. Lee, D. C.; Robel, I.; Pietryga, J. M.; Klimov, V. I. Infrared-Active Heterostructured Nanocrystals with Ultralong Carrier Lifetimes. *J. Am. Chem. Soc.* **2010**, *132*, 9960–9962.
49. Steckel, J. S.; Zimmer, J. P.; Coe-Sullivan, S.; Stott, N. E.; Bulović, V.; Bawendi, M. G. Blue Luminescence from (CdS)ZnS Core–Shell Nanocrystals. *Angew. Chem., Int. Ed.* **2004**, *43*, 2154–2158.
50. Diaconescu, B.; Padilha, L. A.; Nagpal, P.; Swartzentruber, B. S.; Klimov, V. I. Measurement of Electronic States of PbS Nanocrystal Quantum Dots Using Scanning Tunneling Spectroscopy: The Role of Parity Selection Rules in Optical Absorption. *Phys. Rev. Lett.* **2013**, *110*, 127406.